Comparison of Different Strategies to Reduce Acetate Formation in *Escherichia coli*

Marjan De Mey,*,† Gaspard J. Lequeux,‡ Joeri J. Beauprez,† Jo Maertens,‡ Ellen Van Horen,† Wim K. Soetaert,† Peter A. Vanrolleghem,‡ and Erick J. Vandamme†

Ghent University, Laboratory of Industrial Microbiology and Biocatalysis, Department of Biochemical and Microbial Technology, and BIOMATH, Department of Applied Mathematics, Biometrics and Process Control, Faculty of Bioscience Engineering, Coupure Links 653, B-9000 Ghent, Belgium

E. coli cells produce acetate as an extracellular coproduct of aerobic cultures. Acetate is undesirable because it retards growth and inhibits protein formation. Most process designs or genetic modifications to minimize acetate formation aim at balancing growth rate and oxygen consumption. In this research, three genetic approaches to reduce acetate formation were investigated: (1) direct reduction of the carbon flow to acetate (*ackA-pta*, *poxB* knock-out); (2) anticipation on the underlying metabolic and regulatory mechanisms that lead to acetate (constitutive *ppc* expression mutant); and (3) both (1) and (2). Initially, these mutants were compared to the wild-type *E. coli* via batch cultures under aerobic conditions. Subsequently, these mutants were further characterized using metabolic flux analysis on continuous cultures. It is concluded that a combination of directly reducing the carbon flow to acetate and anticipating on the underlying metabolic and regulatory mechanism that lead to acetate, is the most promising approach to overcome acetate formation and improve recombinant protein production. These genetic modifications have no significant influence on the metabolism when growing the microorganisms under steady state at relatively low dilution rates (less than 0.4 h^{-1}).

Introduction

E. coli cells produce acetate as an extracellular coproduct of aerobic cultivations under excess-glucose conditions. This phenomenon is referred as overflow metabolism. Acetate is undesirable because it retards growth even at concentrations as low as 0.5 g/L (*1*) and inhibits protein formation (*2*). Most process designs or genetic modifications to overcome acetate formation ultimately aim to balance growth rate and oxygen consumption (*3*).

Process improvement approaches involve designing growth media or conditions that eliminate or reduce acetate formation. In contrast, genetic approaches involve altering the genetic profile of the strain itself, to restrict the biochemical synthesis of acetate. Process approaches generally focus on reducing the carbon flux entering in the cells and thus diminish the specific growth rate and efficiency of the production process.

For these reasons, our research focuses on genetic approaches to overcome acetate formation. Several interrelated methods have been used to reduce acetate formation genetically. The three partially overlapping strategies are (1) approaches that directly reduce glucose consumption, (2) approaches that directly reduce carbon flow to acetate, and (3) approaches that address underlying metabolic and regulatory mechanisms leading to acetate formation.

* To whom correspondence should be addressed. Tel.: +32-9-264-60-28. Fax: +32-9-264-62-31. E-mail: marjan.demey@ugent.be. Website: http://www.limab.UGent.be.

† Laboratory of Industrial Microbiology and Biocatalysis, Department of Biochemical and Microbial Technology.

‡ BIOMATH, Department of Applied Mathematics, Biometrics and Process Control.

Because the first strategy is a genetic equivalent of bioprocess approaches, this research focuses on the two other strategies based on metabolic modeling and engineering.

Materials and Methods

Bacterial Strains. *Escherichia coli* MG1655 [λ^-, F^-, *rph*-1, *rfb*-50, *ilvG*$^-$] was obtained from The Netherlands Culture Collection of Bacteria (NCCB). *Escherichia coli* MG1655 Δ*ackA-pta*, Δ*poxB* [λ^-, F^-, *rph*-1, *rfb*-50, *ilvG*$^-$, Δ*ackA-pta*, Δ*poxB*] was constructed in the Laboratory of Genetics and Microbiology (MICR) using the method as described by Datsenko and Wanner (2000) (*4*). *Escherichia coli* MG1655 Δ*pppc ppc*-p37 [λ^-, F^-, *rph*-1, *rfb*-50, *ilvG*$^-$, Δ*pppc ppc*-p37], *Escherichia coli* MG1655 Δ*pppc ppc*-p55 [λ^-, F^-, *rph*-1, *rfb*-50, *ilvG*$^-$, Δ*pppc ppc*-p55], *Escherichia coli* MG1655 Δ*ackA-pta*, Δ*poxB*, Δ*pppc ppc*-p37 [λ^-, F^-, *rph*-1, *rfb*-50, *ilvG*$^-$,Δ*ackA-pta*, Δ*poxB*, Δ*pppc ppc*-p37], and *Escherichia coli* MG1655 Δ*ackA-pta*, Δ*poxB*, Δ*pppc ppc*-p55 [λ^-, F^-, *rph*-1, *rfb*-50, *ilvG*$^-$, Δ*ackA-pta*, Δ*poxB*, Δ*pppc ppc*-p55] were constructed in the Laboratory of Genetics and Microbiology (MICR, VUB, Belgium).

Media. The culture medium Luria Broth (LB) consisted of 1% tryptone−peptone (Difco, Erembodegem, Belgium), 0.5% yeast extract (Difco, Erembodegem, Belgium), and 0.5% sodium chloride (VWR, Leuven, Belgium). The pH of the medium was 6.7.

For flask cultures, minimal medium (MM-flask) consisted of 18 μM $FeCl_2 \cdot 4H_2O$ (Merck, Leuven, Belgium), 34 μM $CaCl_2 \cdot 2H_2O$ (Merck, Leuven, Belgium), 8.3 μM $MnCl_2 \cdot 2H_2O$ (Merck, Leuven, Belgium), 2.2 μM $CuCl_2 \cdot 2H_2O$ (Sigma, Bornem, Belgium), 2.1 μM $CoCl_2 \cdot 6H_2O$ (Merck, Leuven, Belgium), 6.9 μM $ZnCl_2$ (Merck, Leuven, Belgium),

10.1021/bp070170g CCC: $37.00
Published on Web 08/23/2007

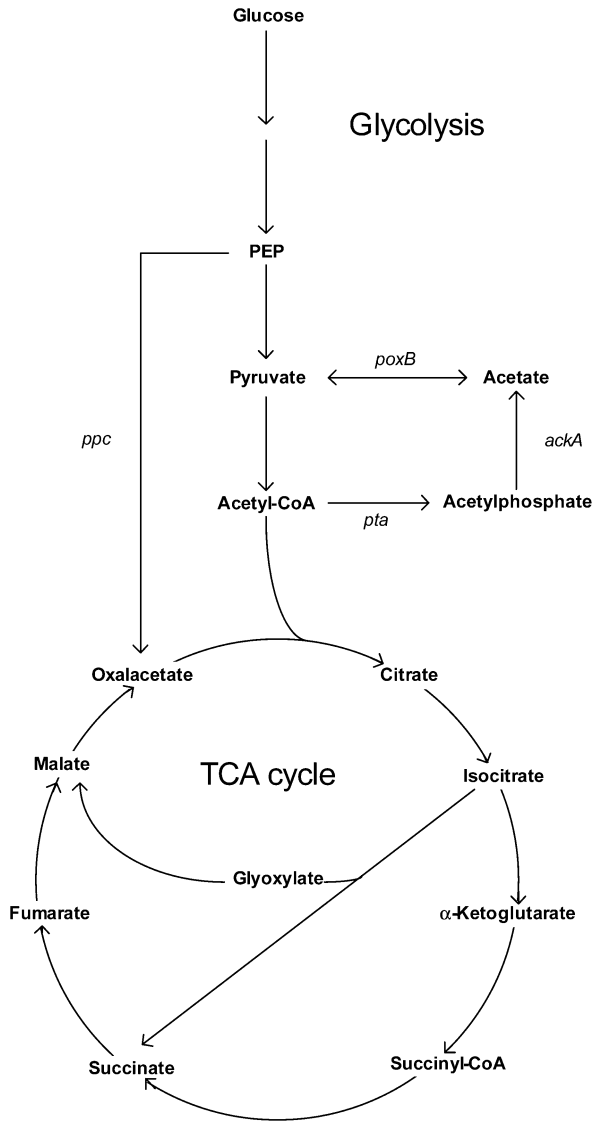

Figure 1. The central metabolism of *Escherichia coli*. PEP, phosphoenolpyruvate; *ackA*, acetate kinase; *poxB*, pyruvate oxidase; *ppc*, phosphoenolpyruvate carboxylase; *pta*, acetylphosphotransferase.

0.4 μM H_3BO_4 (Merck, Leuven, Belgium), 40.3 μM $Na_2EDTA\cdot 2H_2O$ (Fluka, Bornem, Belgium), 3 μM thiamine·HCl (Sigma, Bornem, Belgium), 0.4 μM $Na_2MoO_4\cdot 2H_2O$ (Fluka, Bornem, Belgium), 37.4 mM NH_4Cl (Merck, Leuven, Belgium), 37.8 mM $(NH_4)_2SO_4$ (Merck, Leuven, Belgium), 22 mM KH_2PO_4 (Across), 42 mM KH_2PO_4 (Acros, Geel, Belgium), 40 mM MOPS (Sigma, Bornem, Belgium), 2 mM $MgSO_4\cdot 7H_2O$ (Fluka, Bornem, Belgium), 8.6 mM NaCl (VWR, Leuven, Belgium), and 83.3 mM glucose·H_2O (Cargill). The pH was set at 7.0 with a 1 M K_2HPO_4 (Acros, Geel, Belgium) solution.

For bioreactor cultures, minimal medium (MM-bioreactor) consisted of 18 μM $FeCl_2\cdot 4H_2O$ (Merck, Leuven, Belgium), 34 μM $CaCl_2\cdot 2H_2O$ (Merck, Leuven, Belgium), 8.3 μM $MnCl_2\cdot 2H_2O$ (Merck, Leuven, Belgium), 2.2 μM $CuCl_2\cdot 2H_2O$ (Sigma, Bornem, Belgium), 2.1 μM $CoCl_2\cdot 6H_2O$ (Merck, Leuven, Belgium), 6.9 μM $ZnCl_2$ (Merck, Leuven, Belgium), 0.4 μM H_3BO_4 (Merck, Leuven, Belgium), 40.3 μM $Na_2EDTA\cdot 2H_2O$ (Fluka, Bornem, Belgium), 3 μM thiamine·HCl (Sigma, Bornem, Belgium), 0.4 μM $Na_2MoO_4\cdot 2H_2O$ (Fluka, Bornem, Belgium), 37.4 mM NH_4Cl (Merck, Leuven, Belgium), 37.8 mM $(NH_4)_2SO_4$ (Merck, Leuven, Belgium), 14.7 mM KH_2PO_4 (Acros, Geel, Belgium), 2 mM $MgSO_4\cdot 7H_2O$ (Fluka, Bornem, Belgium), 8.6 mM NaCl (VWR, Leuven, Belgium), and 83.3 mM glucose·H_2O (Cargill). pH was not set to 7.0, but was left at approximatively 5.4.

Inoculum Preparation. A preculture from one colony on a LB-plate in 5 mL LB was grown during 8 h at 37 °C on an orbital shaker at 200 rpm. From the preculture, 2 mL was transferred to 100 mL of MM-flask medium in a 0.5 L shake flask and incubated overnight (16 h) at 37 °C on an orbital shaker at 250 rpm. Subsequently, the inoculum was set at $OD_{600} = 5$ and was 20% of the bioreactor working volume. The inoculum was injected into the vessel with a sterile syringe through an inoculation port sealed with a septum.

Cultivations. All batch fermentations were carried out in a Biostat M culture vessel (Sartorius-BBI Systems, Melsungen, Germany) with a maximum working volume of 1.5 L. Temperature (37 °C), pH (7.0), stirring rate (750 rpm), and airflow rate (1.5 L/min) were controlled by the Biostat M control unit. For maintaining the pH at 7.0, 0.1 N H_2SO_4 (VWR, Leuven, Belgium), and 2 N KOH (Sigma, Bornem, Belgium) were used. Gas that exits the bioreactor passed through an exhaust cooler (Thermostat DC1 equipped with cooler K20, Haake, Karlsruhe, Germany) set at 4 °C before reaching a flask with 0.1 L 10 N NaOH.

Carbon limited continuous cultures were performed in 2 L Biostat B culture vessels (Sartorius-BBI Systems, Melsungen, Germany) with 1.5 L working volume. The operation conditions temperature (37 °C), pH (7.0), stirring rate (600 rpm), and airflow rate (1.5 L/min) were controlled remotely using MFCS/win of Sartorius, a software program associated to the Biostat B Unit. For maintaining the pH at 7.0, 0.1 N H_2SO_4 (VWR, Leuven, Belgium) and 2 N KOH (Sigma, Bornem, Belgium) were used. Gas that exits the bioreactor passed through an exhaust cooler (Thermostat DC1 equipped with cooler K20, Haake, Karlsruhe, Germany) set at 4 °C. O_2 and CO_2 contents in the off gas were measured by a URAS 10E off-gas analyzer from Hartmann and Braun. Two balances were also connected to the computer, one monitoring the influent vessel and one the effluent vessel, allowing precise measurement of the feed rate during chemostat operation.

To avoid foaming, a solution of 10% silicone antifoaming agent (BDH 331512K, VWR Int. Ltd., Poole, England) was added to the culture vessel.

Sampling of the Bioreactor. In its interior, the bioreactor contains a harvest pipe which exits the vessel through a sampling port. The harvest sampling pipe consists of a Bio-Rad HPLC tubing (Bio-Rad, Eke, Belgium). Outside the vessel, the sampling pipe is connected to a Masterflex 16 tubing (Cole Parmer, Antwerpen, Belgium) that creates a circuit back to the vessel and that includes a harvest port with a septum for sampling. The system has been designed to obtain a low retention time of the culture broth in the tubing; on average the broth takes 0.33 s to reach the harvest port and 6 s to go back into the vessel. Such a sampling system is required to have a reliable method for the rapid arrest of cellular metabolism for extracellular metabolite quantification. This system is referred as "rapid sampling loop".

To stop the metabolism of cells during the sampling of the bioreactor, a system using cold stainless steel beads (*5*−*7*) has been used, immediately followed by cold centrifugation (15 000 g, 5 min, 4 °C).

During batch experiments, a sample for OD_{600} and extracellular measurements was taken each hour using the rapid sampling loop and the cold stainless bead sampling method. During exponential growth a sample was taken every 30 min.

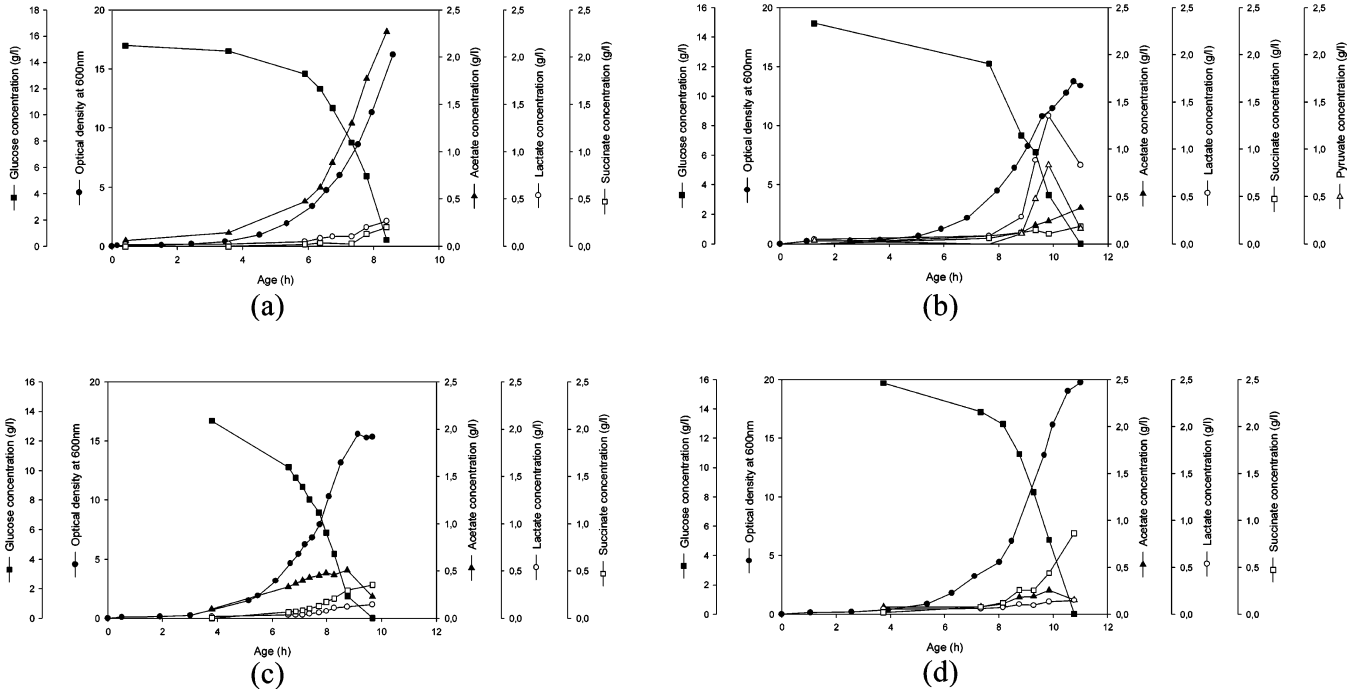

Figure 2. Evolution of biomass and extracellular metabolites during an aerobic batch culture of (a) WT, (b) 3KO, (c) PPC, and (d) 3KO-PPC.

During chemostat experiments, the culture was followed by measuring OD_{600}, extracellular metabolites and cell dry weight. Samples for MFA were taken after the cells attained steady-state, which required at least five residence times, without significant perturbations. Six different samples were taken for extracellular metabolites measurements and five for cell dry weight determination.

Cell Dry Weight. The cell density of the cultures was determined by measuring optical density at 600 nm using a Uvikom 922 spectrophotometer (BRS, Brussel, Belgium). Because of linearity, samples were diluted with physiological solution (0.9% NaCl) when the OD_{600} was above 1. Cell dry weight was obtained by centrifugation (15 min, 5000 g, 4 °C) of 20 g of cell suspension in predried and weighed falcons tubes. The pellets were subsequently washed once with 20 g of physiological solution (0.9% NaCl) and dried at 70 °C to a constant weight. Before each weighing, the falcon tubes were allowed to cool in a desiccator.

Data Analysis. Glucose and organic acids were determined by high performance liquid chromatography (HPLC) on a Varian Prostar HPLC system (Varian, Sint−Katelijne−Waver, Belgium), using an Aminex HPX-87H column (Bio-Rad, Eke, Belgium) equipped with a 1 cm reversed phase precolumn, with 5 mM H_2SO_4 (0.6 mL/min) as mobile phase and heated at 65 °C. Detection was done by a dual-wave UV−vis (210 and 265 nm) detector (Varian Prostar 325) and a differential refractive index detector (MERCK LaChrom L-7490, Merck, Leuven, Belgium).

The phosphate determination method is based on the formation of a phosphomolybdate complex which absorbs at 820 nm (*8*−*10*). First the sample is deproteinised by adding 100 μL of 0.6 N perchloric acid (VWR, Leuven, Belgium) to 100 μL of sample and diluted by adding 800 μL of 0.1 N sodium acetate (VWR, Leuven, Belgium). A total of 300 μL of diluted and deproteinised sample was added to 700 μL of acorbate/molybdate solution (one part 10% ascorbate and six parts 0.42% ammonium molybdate in 1 N H_2SO_4). The reaction mixture was incubated for 20 min at 60 °C. To stop the reaction, 500 μL of "stop solution" (2% sodium citrate tribasic dehydrate, 2% acetic acid) was added to 500 μL of reaction mixture. The absorbance at 820 nm was measured in a microplate reader (680 XR microplate reader, Bio-Rad, Eke, Belgium). For each batch of measurements a calibration curve was made using a stock solution of 1 M KH_2PO_4 (Sigma, Bornem, Belgium). This stock solution was diluted to a concentration of 0.002 M KH_2PO_4 and standard series from 0 to 0.002 M were made for calibration.

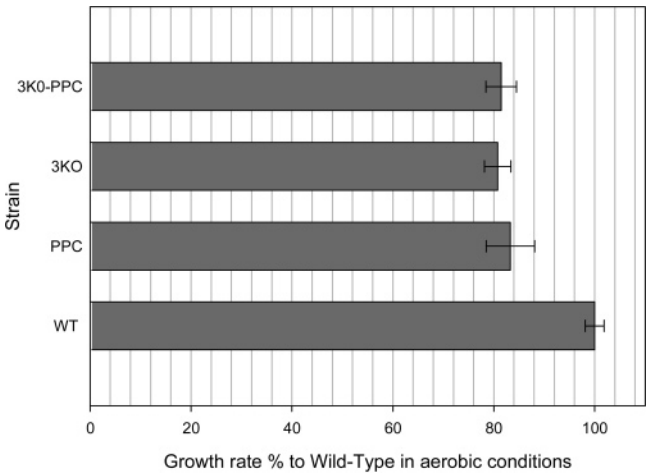

Figure 3. Growth rate (% to *E. coli* MG1655) in aerobic conditions on glucose limiting minimal medium for different strains. Error bars represent the standard deviation.

Quantification of nitrogen in the culture medium was performed using the kit LCK238 from HACH Lange GmbH (Mechelen, Belgium) as described by the supplier.

Metabolic Modeling. The theory behind the MFA techniques used is explained in Lequeux et al. (*11*). Solving and performing the statistical tests on the metabolic models was implemented in SciLab (www.scilab.org). Postprocessing was done using a combination of R (www.r-project.org), xfig (www.xfig.org), and Latex (www.latex-project.org). All fluxes were expressed in mol L^{-1} h^{-1} and model calculations were performed with those units.

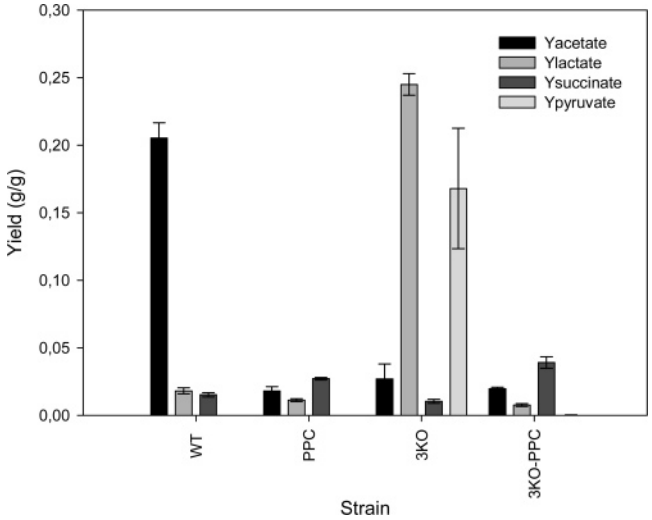

Figure 4. Metabolite yields (g/g) of acetate, lactate, succinate, and pyruvate for different *E. coli* strains during a batch experiment in aerobic conditions on glucose limiting minimal medium. Error bars represent the standard deviation.

Table 1. Dilution Rate *D* (h^{-1}) for the Different Chemostat Experiments

strain	D (h^{-1})
E. coli MG1655	
experiment 1	0.0587 ± 0.0004
experiment 2	0.143 ± 0.00
experiment 3	0.227 ± 0.0016
E. coli MG1655 Δ*ackA*−*pta*, Δ*poxB*	
experiment 1	0.0648 ± 0.0006
experiment 2	0.093 ± 0.005
experiment 3	0.257 ± 0.002
E. coli MG1655 Δ*pppc ppc*−p37	
experiment 1	0.128 ± 0.015
experiment 2	0.163 ± 0.019
experiment 3	0.356 ± 0.042
experiment 4	0.403 ± 0.002
E. coli MG1655 Δ*ackA*−*pta*, Δ*poxB* Δ*pppc ppc*−p37	
experiment 1	0.1137 ± 0.0003
experiment 2	0.1450 ± 0.0003
experiment 3	0.350 ± 0.001

The metabolic model (for details see Tables 2 and 3) included glycolysis, with glucose transported by the PTS system (*12*), the pentose phosphate pathway, and the Krebs cycle.

It is generally assumed that the glyoxylate pathway is not active in the *E. coli* K12 family (from which the strain used in this study is a member) if glucose is provided as a carbon source (*13*, *14*). Instead PEP carboxylase (coded by the gene *ppc*) was used as regenerating reaction for the Krebs cycle metabolites (*15*, *16*). The difference between both pathways is that PEP carboxylase uses one more ATP (*16*).

For every amino acid and nucleotide, the anabolic reactions were included. To avoid parallel pathways (and, thus, parts of the model that cannot be solved), no "salvage" pathways were used. Biosynthesis of LPS, lipid A, peptidoglycane, and the lipid bilayer were also added. The *P*/*O* ratio was set to 1.33 (*17*).

A constant biomass composition was used for every dilution rate: 55% protein, 20.5% RNA, 3.1% DNA, 11.1% lipids, 4.2% LPS, 3.1% peptidoglycane, and 3.1% glycogene (*18*). This resulted in a biomass composition of $C_1H_{1.63}O_{0.392}N_{244}P_{0.021}S_{0.006}$, with molecular mass of 24.16 g/mol.

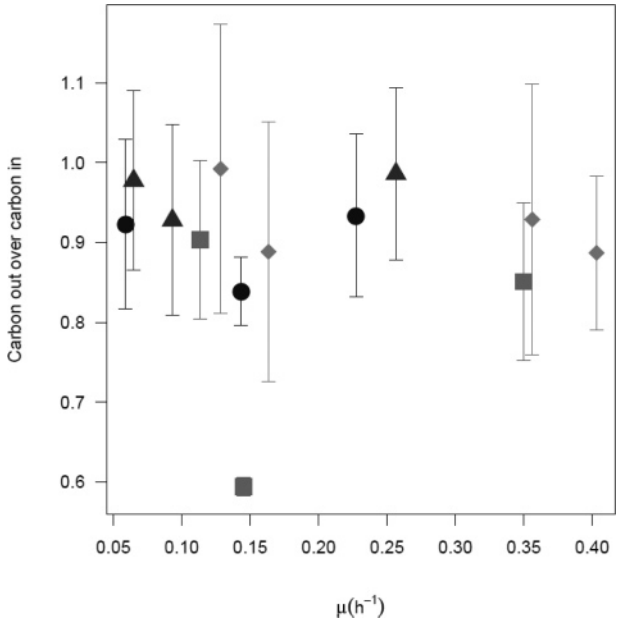

Figure 5. Ratio of carbon out over carbon in. Error bars represent the standard deviation. WT = dot; 3KO = triangle; PPC = diamond; 3KO-PPC = square.

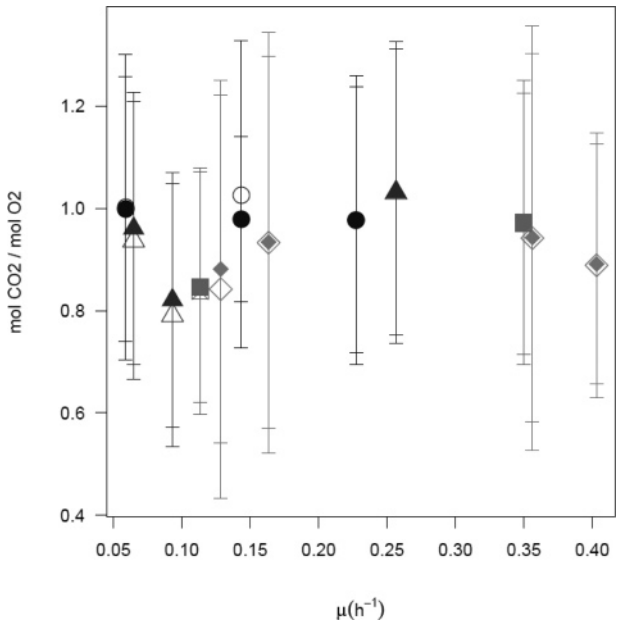

Figure 6. Respiration coefficients. Open symbols stand for the measured values; solid symbols stand for the corrected values by the model. The error bars represent the standard deviation. WT = dot; 3KO = triangle; PPC = diamond; 3KO-PPC = square.

Sources for the reactions were mainly (1) the ecocyc database (*19*−*25*) (http://www.ecocyc.org/); (2) the University of California database (*26*) (http://systemsbiology.ucsd.edu/organisms/ecoli.html); and (3) the KEGG database (*27*, *28*) (http://www.genome.ad.jp/kegg/).

The model contains 137 reactions and 151 metabolites of which 11 were considered exchangeable with the environment: NH_3, PiOH, Biom, GLC, Lac, OAA, Suc, O_2, CO_2, H_2O, H_2SO_4. All parallel pathways were removed. There were no dead-end reactions, and the elemental consistency test was successfully passed (*29*).

Eight metabolites were analyzed for: GLC, NH_3, PiOH, Biom, O_2, CO_2, Lac, and Suc. The model contains 143 independent equations and 137 + 11 = 148 unknown fluxes.

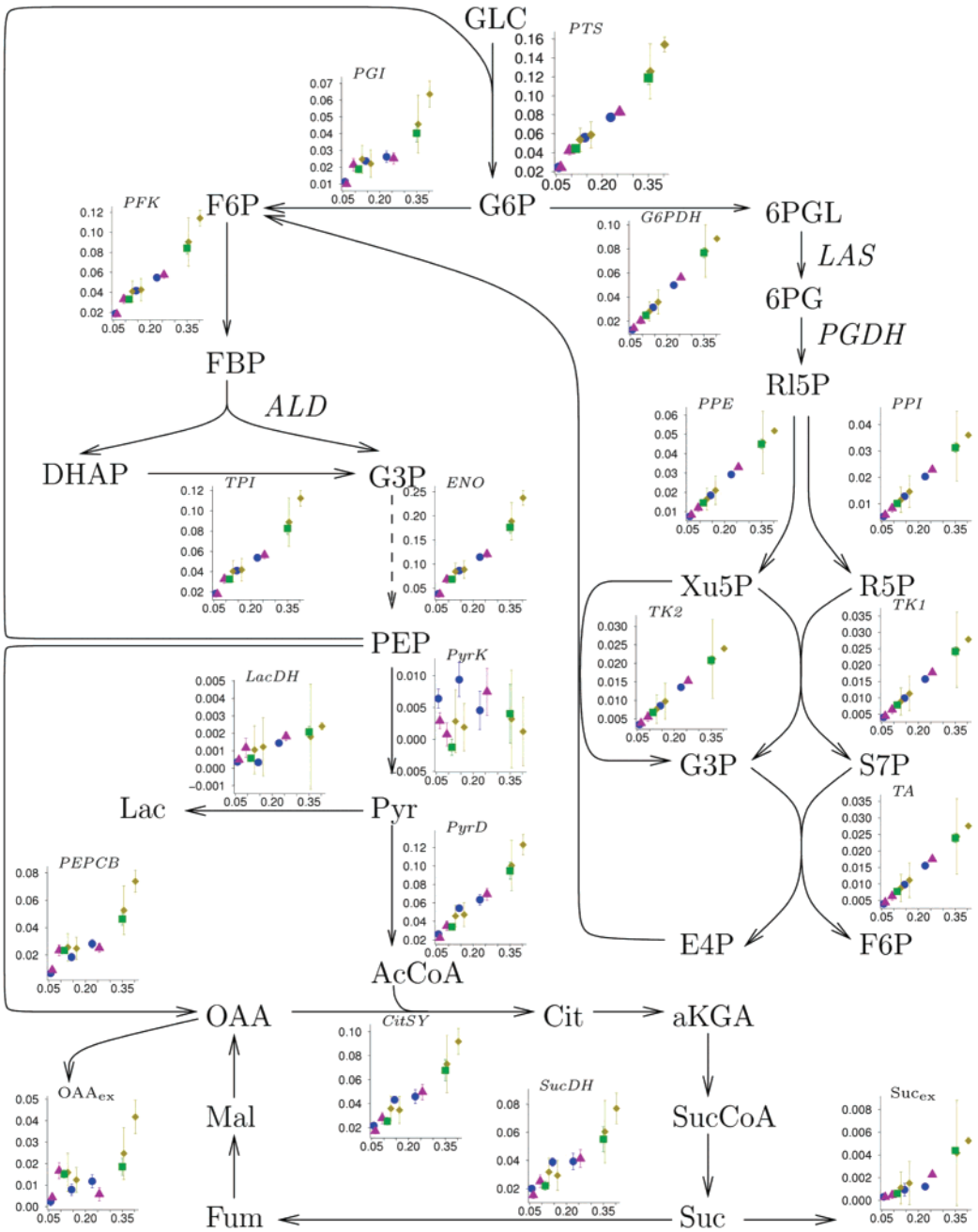

Figure 7. Relative fluxes to biomass (mol/mol Biomass/h) in the glycolysis, the pentose−phosphate pathway, the TCA cycle, and the fermentation pathway. WT = blue dot; 3KO = mauve triangle; PPC = yellow diamond; 3KO-PPC = green square.

Thus, at least five measurements should be performed to solve the model. Hence, three extra measurements were available to run the vector comparison test to detect and remove erroneous measurements (*11*).

Results and Discussion

Even under aerobic conditions, when glucose is excessively present, *E. coli* cells produce acetate as an extracellular byproduct. Acetate is unwanted because it slows down growth and it has a negative effect on recombinant protein production.

Figure 1 depicts the central metabolism of *Escherichia coli*. A first genetic approach to minimize acetate formation is to cut off the flow of carbon to acetate. To achieve this, an *ackA-ptA*, *poxB* knock-out strain (3KO) was created.

A second strategy to reduce acetate formation involves addressing the underlying biochemical mechanisms that lead to acetate. Recent results have potentially elucidated the metabolic and regulatory causes of acetate formation and the links between acetate formation and recombinant protein production. Of the amino acids that ultimately combine to form the protein product, 10 are biochemically derived from TCA cycle metabolites, 11 from glycolysis metabolites and 4 are derived from the pentose phosphate pathway. An important fact is that when *E. coli* is grown in a medium with glucose as the sole carbon source, nearly all the carbon used to synthesize the 10 amino acids derived from TCA metabolites must flow through the anaplerotic pathway mediated by the enzyme phosphoenolpyruvate carboxylase (*3*). In addition, glycolysis and TCA cycle both generate the reduced cofactor $NADH+H^+$. In an aerobic environment, $NADH+H^+$ can be reoxidized to NAD^+, which is necessary to drive the glycolysis and the TCA cycle. The rate at which $NADH+H^+$ is formed proportionally increases with the rate of glucose consumption. However, the specific oxygen uptake rate will reach a plateau when the

Table 2. List of Reactions

PGI	G6P ↔ F6P
PFK	ATP + F6P → ADP + FBP
ALD	FBP ↔ G3P + DHAP
TPI	DHAP ↔ G3P
G3PDH	PiOH + NAD + G3P ↔ NADH + H + BPG
PGK	ADP + BPG ↔ ATP + 3PG
PGM	3PG ↔ 2PG
ENO	2PG ↔ H2O + PEP
PyrK	ADP + PEP → ATP + Pyr
PyrD	NAD + Pyr + CoA → NADH + H + AcCoA + CO_2
CitSY	H2O + AcCoA + OAA → CoA + Cit
ACO	Cit ↔ iCit
CitDH	NAD + iCit ↔ NADH + H + CO_2 + aKGA
AKGDH	NAD + CoA + aKGA → NADH + H + CO_2 + SucCoA
SucCoASY	ADP + PiOH + SucCoA ↔ ATP + CoA + Suc
SucDH	FAD + Suc → $FADH_2$ + Fum
FumHY	H_2O + Fum ↔ Mal
MalDH	NAD + Mal ↔ NADH + H + OAA
PEPCB	H_2O + PEP + CO_2 → PiOH + OAA
LacDH	NADH + H + Pyr ↔ NAD + Lac
PFLY	Pyr + CoA → AcCoA + FA
AcKNLR	ADP + PiOH + AcCoA ↔ ATP + CoA + Ac
Resp	1.33ADP + 1.33PiOH + NADH + H + 0.5O_2 → 1.33ATP + NAD + 2.33H_2O
H_2CO_3SY	H_2O + CO_2 ↔ H2CO3
G6PDH	NADP + G6P → NADPH + H + 6PGL
LAS	H_2O + 6PGL → 6PG
PGDH	NADP + 6PG → NADPH + H + CO_2 + Rl5P
PPI	Rl5P ↔ R5P
PPE	Rl5P ↔ Xu5P
TK1	R5P + Xu5P ↔ G3P + S7P
TA	G3P + S7P ↔ F6P + E4P
TK2	Xu5P + E4P ↔ F6P + G3P
PTS	GLC + PEP → G6P + Pyr
PPiOHHY	PPiOH + H_2O → 2PiOH
GluDH	NADPH + H + aKGA + NH_3 ↔ NADP + H_2O + Glu
GluLI	ATP + NH_3 + Glu → ADP + PiOH + Gln
AspSY	ATP + H_2O + Asp + Gln → AMP + PPiOH + Asn + Glu
AspTA	OAA + Glu ↔ aKGA + Asp
AlaTA	Pyr + Glu ↔ aKGA + Ala
ValAT	aKIV + Glu ↔ aKGA + Val
LeuSYLR	NAD + H_2O + AcCoA + aKIV + Glu → NADH + H + CoA + CO_2 + aKGA + Leu
aKIVSYLR	NADPH + H + 2Pyr → NADP + H_2O + CO_2 + aKIV
IleSYLR	NADPH + H + Pyr + Glu + Thr → NADP + H_2O + CO_2 + aKGA + NH_3 + Ile
ProSYLR	ATP + 2NADPH + 2H + Glu → ADP + PiOH + 2NADP + H_2O + Pro
SerLR	NAD + H_2O + 3PG + Glu → PiOH + NADH + H + aKGA + Ser
SerTHM	Ser + THF → H_2O + Gly + MeTHF
H2SSYLR	2ATP + 3NADPH + $ThioredH_2$ + 3H + H_2SO_4 → ADP + PPiOH + 3NADP + Thiored + 3H_2O + H_2S + PAP
PAPNAS	H_2O + PAP → AMP + PiOH
CysSYLR	H_2S + AcCoA + Ser → CoA + Cys + Ac
PrppSY	ATP + R5P → AMP + PRPP
HisSYLR	ATP + 2NAD + 3H_2O + Gln + PRPP → 2PPiOH + PiOH + 2NADH + 2H + aKGA + His + AICAR
PheSYLR	Glu + Chor → H_2O + CO_2 + aKGA + Phe
TyrSYLR	NAD + Glu + Chor → NADH + H + CO_2 + aKGA + Tyr
TrpSYLR	Gln + Ser + Chor + PRPP → PPiOH + 2H_2O + G3P + Pyr + CO_2 + Glu + Trp
DhDoPHepAD	H_2O + PEP + E4P → PiOH + Dahp
DhqSY	Dahp → PiOH + Dhq
DhsSYLR	Dhq ↔ H_2O + Dhs
ShiSY	NADPH + H + Dhs ↔ NADP + Shi
ShiKN	ATP + Shi → ADP + Shi3P
ChorSYLR	PEP + Shi3P → 2PiOH + Chor
ThrSYLR	ATP + H_2O + HSer → ADP + PiOH + Thr
MDAPSYLR	ADPH + H + Pyr + SucCoA + Glu + AspSA → NADP + CoA + aKGA + Suc + MDAP
LysSY	MDAP → CO_2 + Lys
MetSYLR	H_2O + SucCoA + Cys + MTHF + HSer → Pyr + CoA + Suc + NH_3 + Met + THF
ArgSYLR	ATP + Asp + Orn + CarP → AMP + PPiOH + PiOH + Fum + Arg
ThioredRD	NADPH + Thiored + H ↔ NADP + $ThioredH_2$
H_2O_2ox	2H_2O_2 → 2H_2O + O_2
FAD2NAD	NAD + FADH2 ↔ NADH + FAD + H
AICARSYLR	6ATP + 3H_2O + CO_2 + Asp + 2Gln + Gly + FA + PRPP → 6 ADP + PPiOH + 6PiOH + Fum + 2Glu + AICAR
IMPSYLR	FTHF + AICAR → H_2O + THF + IMP
AMPSYLR	Asp + GTP + IMP → AMP + PiOH + Fum + GDP
AdKN	ATP + AMP ↔ 2ADP
ADPRD	ADP + $ThioredH_2$ → Thiored + H_2O + dADP
dADPKN	ATP + dADP → ADP + dATP
IMPDH	NAD + H_2O + IMP → NADH + H + XMP
GMPSY	ATP + H_2O + Gln + XMP → AMP + PPiOH + Glu + GMP
GuKN	ATP + GMP → ADP + GDP
GDPKN	ATP + GDP → ADP + GTP
GDPRD	$ThioredH_2$ + GDP → Thiored + H_2O + dGDP
dGDPKN	ATP + dGDP → ADP + dGTP
UMPSYLR	O_2 + Asp + PRPP + CarP → PPiOH + PiOH + H_2O + CO_2 + UMP + H_2O_2
UrKN	ATP + UMP → ADP + UDP
UDPKN	ATP + UDP → ADP + UTP
CTPSY	ATP + H_2O + Gln + UTP → ADP + PiOH + Glu + CTP
CDPKN	ATP + CDP ↔ ADP + CTP
CMPKN	ATP + CMP → ADP + CDP
CDPRD	$ThioredH_2$ + CDP → Thiored + H_2O + dCDP
dCDPKN	ATP + dCDP → ADP + dCTP
UDPRD	$ThioredH_2$ + UDP → Thiored + H_2O + dUDP
dUDPKN	ATP + dUDP → ADP + dUTP
dUTPPPAS	H_2O + dUTP → PPiOH + dUMP
dTMPSY	MeTHF + dUMP → DHF + dTMP
dTMPKN	ATP + dTMP → ADP + dTDP
dTDPKN	ATP + dTDP → ADP + dTTP
DHFRD	NADPH + H + DHF → NADP + THF
FTHFSYLR	NADP + H_2O + MeTHF → NADPH + H + FTHF
GlyCA	NAD + Gly + THF ↔ NADH + H + CO_2 + NH_3 + MeTHF
MeTHFRD	NADH + H + MeTHF → NAD + MTHF
AcCoACB	ATP + H_2O + AcCoA + CO_2 ↔ ADP + PiOH + MalCoA
MalCoATA	MalCoA + ACP ↔ CoA + MalACP
AcACPSY	MalACP → CO_2 + AcACP
C120SY	10NADPH + 10H + AcACP + 5MalACP → 10NADP + 5H_2O + 5CO_2 + C120ACP + 5ACP
C140SY	12NADPH + 12H + AcACP + 6MalACP → 12NADP + 6H_2O + 6CO_2 + C140ACP + 6ACP
C160SY	14NADPH + 14H + AcACP + 7MalACP → 14NADP + 7H_2O + 7 CO_2 + C160ACP + 7ACP
C181SY	15NADPH + 15H + AcACP + 8MalACP → 15NADP + 8H_2O + 8CO_2 + C181ACP + 8ACP
AcylTF	C160ACP + C181ACP + Go3P → 2ACP + PA
Go3PDH	NADPH + H + DHAP ↔ NADP + Go3P
DGoKN	ATP + DGo → ADP + PA
CDPDGoSY	CTP + PA ↔ PPiOH + CDPDGo
PSerSY	Ser + CDPDGo → CMP + PSer
PSerDC	PSer → CO_2 + PEthAn
GlnF6PTA	F6P + Gln → Glu + GA6P
GlcAnMU	GA6P ↔ GA1P
NAGUrTF	AcCoA + UTP + GA1P → PPiOH + CoA + UDPNAG
LipaSYLR	ATP + 2CMPKDO + 2UDPNAG + C120ACP + 5C140ACP → ADP + 2CMP + UMP + UDP + 6ACP + Lipa + 2Ac
A5PIR	Rl5P ↔ Ar5P
PGLCMT	G6P ↔ G1P
CMPKDOSYLR	2H_2O + PEP + Ar5P + CTP → PPiOH + 2PiOH + CMPKDO
ADPHEPSY	ATP + S7P → PPiOH + ADPHEP
UDPGlcSY	G1P + UTP → PPiOH + UDPGlc
EthANPT	CMP + PEthAn ↔ CDPEthAn + DGo
LpsSYLR	3ADPHEP + 3CMPKDO + 2UDPGlc + Lipa + 2CDPEthAn → 3ADP + 3CMP + 2CDP + 2UDP + Lps
PGSYLR	Go3P + CDPDGo → PiOH + CMP + PG
CLSY	PG + CDPDGo → CMP + CL
PeptidoSYLR	5ATP + NADPH + H + PEP + 3Ala + MDAP + 2UDPNAG → 5ADP + 7PiOH + NADP + UMP + UDP + Peptido
GlcgSY	ATP + G1P → ADP + PPiOH + Glcg
ATPHY	ATP + H_2O → ADP + PiOH
DNASYLR	2H_2O + 0.246dATP + 0.254dGTP + 0.254dCTP + 0.246dTTP → 2PiOH + DNA

Table 2. (Continued)

AspSASY	ATP + NADPH + H + Asp → ADP + PiOH + NADP + AspSA	RNASYLR	0.262ATP + $2H_2O$ + 0.322GTP + 0.2CTP + 0.216UTP → 2PiOH + RNA
HSerDH	NADPH + H + AspSA ↔ NADP + HSer	ProtSYLR	2ATP + $3H_2O$ + 0.0961Ala + 0.05506Arg + 0.04505Asn + 0.04505Asp + 0.01702Cys + 0.04905Gln + 0.04905Glu + 0.1151Gly + 0.01802His + 0.05405Ile + 0.08408Leu +0.06406Lys + 0.02903Met + 0.03504Phe + 0.04104Pro + 0.04004Ser + 0.04705Thr + 0.01101Trp + 0.02603Tyr + 0.07908Val + 2GTP → 2ADP + 4PiOH + 2GDP + Prot
CarPSY	2ATP + H_2O + H_2CO_3 + Gln → 2ADP + PiOH + Glu + CarP	LipidSYLR	0.0266CL + 0.202PG + 0.7714PEthAn → Lipid
OrnSYLR	ATP + NADPH + H + H_2O + AcCoA + 2Glu → ADP + PiOH + NADP + CoA + aKGA + Orn + Ac	BiomSYLR	0.004561Glcg + 0.0002663Lps + 0.0008933Peptido + 0.002291DNA + 0.01446RNA + 0.1227Prot + 0.003642Lipid → Biom

maximum rate at which *E. coli* can consume oxygen is achieved, despite its availability. At this point, cellular respiration is not able to regenerate sufficient NAD^+, resulting in the accumulation of $NADH+H^+$, which plays an important role in acetate formation. First, $NADH+H^+$ is a strong allosteric inhibitor of the enzyme citrate synthase, which mediates the first step of the TCA cycle. Thus accumulation of $NADH+H^+$ will inhibit the carbon flow to the TCA cycle and consequently decrease the formation of the 10 TCA cycle derived amino acids. Second, the redox ratio ($NADH+H^+/NAD^+$) is involved in the regulation of the ArcA regulatory system in *E. coli*, which represses the expression of several genes in the TCA cycle. *E. coli* will respond to increased $NADH+H^+$ levels by redirecting the carbon flow to acetate production that generates less $NADH+H^+$ (*3*).

A strategy to divert the carbon flow from acetate to the TCA cycle and to produce less $NADH+H^+$ is to overexpress PEP carboxylase encoded by the gene *ppc*. Previous research already indicated that overexpressing *ppc* reduces acetate formation (*30*, *36*). Therefore, a *ppc* overexpressing mutant of *E. coli* was created in which the natural *ppc* promoter was replaced with a strong constitutive artificial promoter (PPC) (*31*). Finally, the two approaches were combined by replacing the natural *ppc* promoter with p37 in *E. coli* Δ*ackA-pta*, Δ*poxB* (3KO-PPC).

Batch Experiments. Different *E. coli* strains were studied, representing different approaches to minimize acetate formation; initially, batch cultures were performed on glucose limiting minimal medium under aerobic conditions with the following strains: *E. coli* MG1655 (WT), *E. coli* MG1655 Δp*ppc ppc*-p37 (PPC), *E. coli* MG1655 Δ*ackA-pta*, Δ*poxB* (3KO), and *E. coli* MG1655 Δ*ackA-pta*, Δ*poxB*, Δp*ppc ppc*-p37 (3KO-PPC).

During the culture, the growth progress (OD_{600}) and extracellular metabolite concentrations were determined. The results are depicted in Figure 2.

From these data, the growth rate (μ) and the relevant metabolite yields (Y metabolite) were determined for the different strains. The μ was calculated by determining the slope of the curve obtained by plotting $\ln(OD_{600})$ in function of the time using the software Sigma-plot 10.0; the metabolite yields were calculated by determining the slope of the curves obtained by plotting the metabolite concentration in the function of the glucose consumption also using Sigma-plot 10.0. The results are given in Figures 3 and 4.

Cutting off the carbon flow to acetate results in a decreased growth rate to 80% as compared to the wild-type. This is caused by the decreased availability of energy as the acetate pathway generates one ATP extra and consumes one more $NADH+H^+$ compared to the lactate pathway (which is used when the acetate pathway is knocked out). The same effect is observed in the *ppc* overexpressing strain. By diverting the carbon flow from phophoenolpyruvate (PEP) to oxaloacetate instead of pyruvate, less PEP is available for the PTS to transport glucose into the cell. In addition, combination of cutting off the carbon flow toward acetate and diverting the carbon flow from PEP toward oxaloacetate has no additional effect.

However, a decrease of 20% in maximal growth rate (as compared to the wild-type) still corresponds to a growth rate of 1.82 h^{-1} and a generation time of 0.38 h, which indicates that these mutant strains remain fast growing and, thus, applicable for large industrial processes.

Figure 4 illustrates that the acetate yield in the wild-type is quite high. Cutting off the carbon flow toward acetate reduces the acetate yield significantly (7.6 times). However the lactate yield increases substantially (13.5 times). This indicates that the genetic approach of interrupting the carbon flow toward acetate results in minimizing acetate. However, other byproducts are formed making this strategy unfavorable. This confirms data found in literature (*32*−*35*). All report a strong reduction of acetate production, when *ackA* and *pta* are eliminated. This is at the expense of the growth rate and is accompanied by an increase in the production of other fermentation products such as lactate and formate.

The genetic approach of redirecting the carbon flow from PEP toward oxaloacetate seems more promising. The acetate yield decreases 11.5 times. The succinate yield on the other hand increases significantly (1.8 times), whereas the lactate yield decreases 1.6 times, indicating an increased flux toward the TCA cycle and thus toward the amino acid precursors. In the literature, overexpression of *ppc* from a plasmid in flask-cultures is described and yields in a reduction of acetate (*36*). In contrast to Farmer and Liao (1997) (*36*), in this contribution, *ppc* is constitutively overexpressed by replacing the natural promoter in the *E. coli* genome. Therefore, this approach introduces minimal changes in the host, is easily applicable to industrial strains, and there is no need for a selection marker (e.g., antibiotic) and an inducer (e.g., IPTG) to maintain the plasmid and to express the gene, respectively, making this approach more favorable.

Combination of the two genetic approaches results in similar fermentation behavior as replacing the natural *ppc* promoter by a strong promoter, except for the succinate yield that increases 2.5 times, as compared to the wild-type; this is significantly higher compared to *E. coli* MG1655 Δp*ppc ppc*-p37.

Considering these results of the batch experiments, it was decided to perform chemostat experiments to elucidate the influence of these genetic manipulations on the central metabolism under chemostat conditions.

Chemostat Experiments and MFA. To collect data for the metabolic steady-state model of *Escherichia coli* MG1655, chemostat experiments were performed with different mutant strains and at minimally three different dilution rates per strain.

The actual dilution rates (*D*) for the different chemostat experiments are given in Table 1.

Table 3. List of Metabolites

2PG	$C_3H_7O_7P$	2-phophoglycerate	Gln	$C_5H_10O_3N_2$	glutamine
3PG	$C_3H_7O_7P$	3-phophoglycerate	Glu	$C_5H_9O_4N$	glutamate
6PG	$C_6H_{13}O_{10}P$	6-phosphogluconate	Gly	$C_2H_5O_2N$	glycine
6PGL	$C_6H_{11}O_9P$	6-phosphogluconolacton	GMP	$C_{10}H_{14}O_8N_5P$	guanosine monophosphate
Ac	$C_2H_4O_2$	acetate	Go3P	$C_3H_9O_6P$	glycerol-3-phosphate
AcACP	C_2H_3OPept	acetyl ACP	GTP	$C_{10}H_{16}O_{14}N_5P_3$	guanosine triphosphate
AcCoA	$C_{23}H_{34}O_{17}N_7P_3S$	acetyl CoA	H	H^+	hydrogene
ACP	HPept	acyl carrier protein	H2CO3	CH_2O_3	bicarbonate
ADP	$C_{10}H_{15}O_{10}N_5P_2$	adenosine diphosphate	H2O	H_2O	water
ADPHEP	$C_{17}H_27O_{16}N_5P_2$	ADP-mannoheptose	H2O2	H_2O_2	water peroxide
AICAR	$C_9H_{15}O_8N_4P$	amino imidazole carboxamide ribonucleotide	H2S	H_2S	hydrogene sulfide
aKGA	$C_5H_6O_5$	alpha keto glutaric acid	H2SO4	H_2O_4S	sulfuric acid
aKIV	$C_5H_8O_3$	alpha-keto-isovalerate	His	$C_6H_9O_2N_3$	histidine
Ala	$C_3H_7O_2N$	alanine	Hser	$C_4H_9O_3N$	homoserine
AMP	$C_{10}H_{14}O_7N_5P$	adenosine monophosphate	iCit	$C_6H_8O_7$	isocitraat
Ar5P	$C_5H_{11}O_8P$	arabinose-5-phosphate	Ile	$C_6H_{13}O_2N$	isoleucine
Arg	$C_6H_{14}O_2N_4$	arginine	IMP	$C_{10}H_{13}O_8N_4P$	inosine monophosphate
Asn	$C_4H_8O_3N_2$	aspartate	Lac	$C_3H_6O_3$	lactate
Asp	$C_4H_7O_4N$	asparagine	Leu	$C_6H_{13}O_2N$	leucine
AspSA	$C_4H_7O_3N$	aspartate semialdehyde	Lipa	$C_{110}H_{196}O_{32}N_2P_2$	lipid A
ATP	$C_{10}H_{16}O_{13}N_5P_3$	adenosine triphosphate	Lipid	$C_{40.2}H_{77.6}O_{8.41}$-$N_{0.771}P_{1.03}$	lipid composition
Biom	$CH_{1.627}O_{0.3915}N_{0.244}$-$P_{0.02102}S_{0.00565}$	biomass	Lps	$C_{171}H_{298}O_{81}N_4P_2$	lipopolysaccharide
BPG	$C_3H_8O_{10}P_2$	1,3-biphosphoglycerate	Lys	$C_6H_{14}O_2N_2$	lysine
C120ACP	$C_{12}H_{23}OPept$		Mal	$C_4H_6O_5$	malate
C140ACP	$C_{14}H_{27}OPept$		MalACP	$C_3H_3O_3Pept$	malonyl ACP
C160ACP	$C_{16}H_{31}OPept$		MalCoA	$C_{24}H_{34}O_{19}N_7P_3S$	malonyl CoA
C181ACP	$C_{18}H_{33}OPept$		MDAP	$C_7H_{14}O_4N_2$	meso-diaminopimelate
CarP	CH_4O_5NP	carbamoyl phosphate	Met	$C_5H_{11}O_2NS$	methionine
CDP	$C_9H_{15}O_{11}N_3P_2$	citidine diphosphate	MeTHF	$C_{20}H_{23}O_6N_7$	methylene tetrahydrofolate
CDPDGo	$C_{46}H_{83}O_{15}N_3P_2$	CDP-diacylglycerol	MTHF	$C_{20}H_{25}O_6N_7$	methyl tetrahydrofolate
CDPEthAn	$C_{11}H_{20}O_{11}N_4P_2$	CDP-ethanolamine	NAD	$C_{21}H_{28}O_{14}N_7P_2^+$	nicotinamide adenine dinucleotide
Chor	$C_{10}H_{10}O_6$	chorismate	NADH	$C_{21}H_{29}O_{14}N_7P_2$	reduced NAD
Cit	$C_6H_8O_7$	cisaconitate	NADP	$C_{21}H_{28}O_{17}N_7P_3^+$	nicotinamide adenine dinucleotide phosphate
CL	$C_{77}H_{144}O_{16}P_2$	cardiolipin	NADPH	$C_{21}H_{29}O_{17}N_7P_3$	reduced NADPH
CMP	$C_9H_{14}O_8N_3P$	citidine monophosphate	NH3	H_3N	ammonia
CMPKDO	$C_{17}H_{26}O_{15}N_3P$	CMP-2-keto-3-deoxyoctanoate	O2	O_2	oxygen
CO2	CO_2	carbon dioxide	OAA	$C_4H_4O_5$	oxaloacetate
CoA	$C_{21}H_{32}O_{16}N_7P_3S$	coenzyme A	Orn	$C_5H_{12}O_2N_2$	ornithine
CTP	$C_9H_{16}O_{14}N_3P_3$	citidine triphosphate	PA	$C_{37}H_{71}O_8P$	phosphatidyl acid
Cys	$C_3H_7O_2NS$	cysteine	PAP	$C_{10}H_{15}O_{10}N_5P_2$	phospho adenosine phosphate
dADP	$C_{10}H_{15}O_9N_5P_2$	deoxy ADP	PEP	$C_3H_5O_6P$	phosphoenolpyruvate
Dahp	$C_7H_{13}O_{10}P$	deoxy arabino heptulosonate	Peptido	$C_{35}H_{53}O_{16}N_7$	peptidoglycane
dATP	$C_{10}H_{16}O_{12}N_5P_3$	deoxy ATP	PEthAn	$C_{39}H_{76}O_8NP$	phosphatidyl ethanolamine
dCDP	$C_9H_{15}O_{10}N_3P_2$	deoxy CDP	PG	$C_{40}H_{75}O_9P$	phosphatidyl glycerol
dCTP	$C_9H_{16}O_{13}N_3P_3$	deoxy CTP	Phe	$C_9H_{11}O_2N$	phenylalanine
dGDP	$C_{10}H_{15}O_{10}N_5P_2$	deoxy GDP	PiOH	H_3O_4P	phosphate
DGo	$C_{37}H_{70}O_5$	diacyl glycerol	PPiOH	$H_4O_7P_2$	pyrophosphate
dGTP	$C_{10}H_{16}O_{13}N_5P_3$	deoxy GTP	Pro	$C_5H_9O_2N$	proline
DHAP	$C_3H_7O_6P$	dihydroxyaceton phosphate	Prot	$C_{4.797}H_{9.667}O_{1.395}$-$N_{1.37}S_{0.04}605$	protein composition
DHF	$C_{19}H_{21}O_6N_7$	dihydrofolate	PRPP	$C_5H_{13}O_{14}P_3$	5-phospho-alpha-D-ribosyl-1-pyrophosphate
Dhq	$C_7H_{10}O_6$	dehydroquinate	PSer	$C_{40}H_{76}O_{10}NP$	phosphatidyl serine
Dhs	$C_7H_8O_5$	dehydroshikimate	Pyr	$C_3H_4O_3$	pyruvate
DNA	$C_{9.75}H_{14.2}O_7N_{3.75}P$	DNA composition	R5P	$C_5H_{11}O_8P$	ribose-5-phosphate
dTDP	$C_{10}H_{16}O_{11}N_2P_2$	deoxy TDP	Rl5P	$C_5H_{11}O_8P$	ribulose-5-phosphate
dTMP	$C_{10}H_{15}O_8N_2P$	deoxy TMP	RNA	$C_{9.58}H_{13.8}O_{7.95}N_{3.95}P$	RNA composition
dTTP	$C_{10}H_{17}O_{14}N_2P_3$	deoxy TTP	S7P	$C_7H_{15}O_{10}P$	sedoheptulose-7-phosphate
dUDP	$C_9H_{14}O_{11}N_2P_2$	deoxy UDP	Ser	$C_3H_7O_3N$	serine
dUMP	$C_9H_{13}O_8N2P$	deoxy UMP	Shi	$C_7H_{10}O_5$	shikimate
dUTP	$C_9H_{15}O_{14}N_2P_3$	deoxy UTP	Shi3P	$C_7H_{11}O_8P$	shikimate-3-phosphate
E4P	$C_4H_9O_7P$	erythrose-4-phosphate	Suc	$C_4H_6O_4$	succinate
F6P	$C_6H_{13}O_9P$	fructose-6-phosphate	SucCoA	$C_{25}H_{36}O_{19}N_7P_3S$	succinyl CoA
FA	CH_2O_2	formic acid	THF	$C_{19}H_{23}O_6N_7$	tetrahydrofolate
FAD	$C_{27}H_{33}O_{15}N_9P_2$	flavine adeninen dinucleotide	Thiored	Pept	thioredoxin
FADH2	$C_{27}H_{35}O_{15}N_9P_2$	reduced FAD	ThioredH2	H_2Pept	Reduced thioredoxin
FBP	$C_6H_{14}O_{12}P_2$	fructose-1,6-biphosphate	Thr	$C_4H_9O_3N$	Threonine
FTHF	$C_{20}H_{23}O_7N_7$	formyl tetrahydrofolate	Trp	$C_{11}H_{12}O_2N_2$	Tryptophan
Fum	$C_4H_4O_4$	fumarate	Tyr	$C_9H_{11}O_3N$	Tyrosine
G1P	$C_6H_{13}O_9P$	glucose-1-phosphate	UDP	$C_9H_{14}O_{12}N_2P_2$	Uridine diphosphate
G3P	$C_3H_7O_6P$	glyceraldehyde-3-phosphate	UDPGlc	$C_{15}H_{24}O_{17}N_2P_2$	UDP glucose
G6P	$C_6H_{13}O_9P$	glucose-6-phosphate	UDPNAG	$C_{17}H_{27}O_{17}N_2P_2$	UDP N-acetyl glucosamine
GA1P	$C_6H_{14}O_8NP$	D-glucosamine-6-phosphate	UMP	$C_9H_{13}O_9N_2P$	Uridine monophosphate
GA6P	$C_6H_{14}O_8NP$	D-glucosamine-6-phosphate	UTP	$C_9H_{15}O_{15}N_2P_3$	Uridine triphosphate
GDP	$C_{10}H_{15}O_{11}N_5P_2$	guanosine diphosphate	Val	$C_5H_{11}O_2N$	Valine
GLC	$C_6H_{12}O_6$	glucose	XMP	$C_{10}H_{13}O_9N_4P$	Xanthosine-5-phosphate
Glcg	$C_6H_{10}O_5$	glycogen	Xu5P	$C_5H_{11}O_8P$	Xylulose-5-phosphate

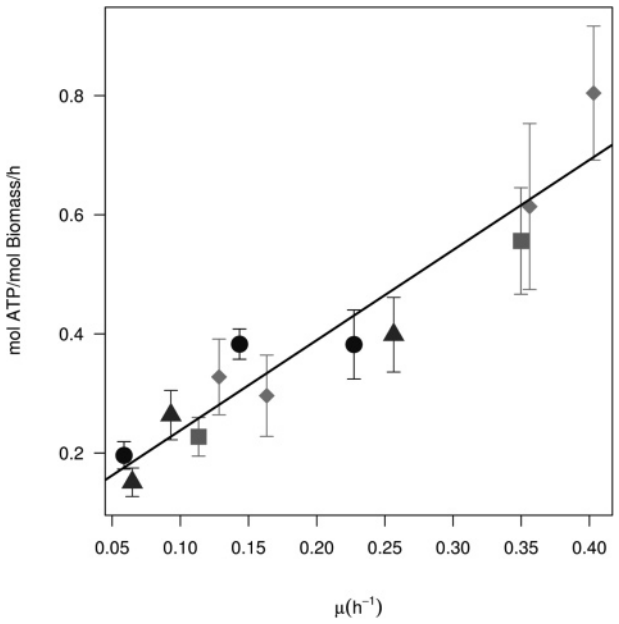

Figure 8. Moles of ATP per mol of biomass per hour that are hydrolyzed for the different strains at different growth rates. WT = dot; 3KO = triangle; PPC = diamond; 3KO-PPC = square.

For each experiment, it was verified whether the culture was C-limited by measuring the residual glucose concentration in the supernatant.

Metabolic flux analysis was performed for further characterization of the different *E. coli* strains.

Data Quality Assessment. To assess the quality of the data, the carbon balance of the different chemostat experiments for the different strains were evaluated (Figure 5). The carbon balance is calculated from the measured fluxes.

Figure 5 shows that two experiments (WT at $D = 0.143\ h^{-1}$ and 3KO-PPC at $D = 0.145\ h^{-1}$) have a carbon balance that significantly does not close. However, the experiment WT at $D = 0.143\ h^{-1}$ was kept in the data set because the absolute error is small even though the coincidental small variance on the measurements makes this error significant. Furthermore, the calculated fluxes were in accordance with those at other dilution rates. Experiment 3KO-PPC at $D = 0.145\ h^{-1}$ was not used in the subsequent calculations: the error on the carbon balance is much larger and the statistical test performed on the model residuals rejected this experiment.

The ratio between the oxygen uptake rate and the carbon dioxide excretion rate is called respiratory quotient (RQ). The RQ of the different chemostat experiments with the different strains are depicted in Figure 6. It can be seen that the RQs do not significantly differ from 1.

For each chemostat, the metabolic model was solved and the statistical test to assess the quality of fit of the model to the data was run. The H0 hypothesis of this test is that the residuals (defined as the measured fluxes minus the model predicted fluxes) are zero (see (*11*) for a detailed discussion of this test). When this test was not passed successfully, the vector comparison test was used to find (and ultimately remove) the wrong measurement.

For four models, the residuals were significantly different from zero: experiment WT at $D = 0.227\ h^{-1}$, 3KO at $D = 0.064\ h^{-1}$, 3KO at $D = 0.256\ h^{-1}$, and 3KO-PPC at $D = 0.145\ h^{-1}$. Subsequently, erroneous measurements were removed.

For WT at $D = 0.227\ h^{-1}$, the NH_3 measurement was removed as suggested by the vector comparison test.

In the case of 3KO at $D = 0.064\ h^{-1}$, the vector comparison test suggested to remove the biomass and CO_2 measurements. Only the biomass measurement had to be removed to make the model being fully accepted.

In the case of 3KO at $D = 0.256\ h^{-1}$, the vector comparison test suggested to remove the NH_3 and PiOH measurements. When these measurements were removed the model was fully accepted.

For 3KO-PPC at $D = 0.145\ h^{-1}$, the model was not accepted and the vector comparison test suggested to remove the NH_3 and the biomass measurements. However, after removing those measurements, the P-value of the χ^2-statistical test for accepatance of the model was still only 0.06. Because of this low P-value and because of the ratio carbon out over carbon in was approxiomately 0.6, it was decided not to take these measurements into account for the further analysis.

MFA Results. Figure 7 depicts the fluxes (expressed in mol/mol biomass/h) in the glycolysis, the pentose−phosphate pathway, the TCA cycle, and the fermentation pathways. The perfect linear relationships for the different dilution rates in the pentose−phosphate pathway originates from the fact that this pathway is under the assumptions of this model, solely used for generating biomass precursors.

Although there appear to be some slight changes in some fluxes, Figure 7 shows that in general no significant difference in the flux map for the different strains can be observed indicating no negative influence of the genetic modifications on primary metabolism.

The biomass yield on glucose is around 0.45 C-mol/C-mol. MFA can quantitatively show where in the central carbon metabolism the carbon is taken out for biomass precursors.

At the G6P node, more than half of the carbon flows toward the pentose−phosphate pathway and not to the glycolysis. However, most of this flows back into the glycolysis as F6P and finally only 15% (taking into account the CO_2 production in the beginning of the PPC) of the glucose is channeled via the PPC to biomass.

The flux of PyrK, converting PEP to pyruvate is essentially zero for all dilution rates. This is in agreement with the results found in Carlson and Srienc (2004) (*37*). They generated potential efficient pathways for biomass production using elementary mode analysis. All those pathways have a very low or zero PyrK flux, which means that all pyruvate originates from PTS.

PyrD only consumes three-fourths of the available pyruvate, the remaining is used for biomass precursor synthesis. Thus, around 13% of the glucose carbon is converted to biomass via pyruvate.

For the fatty acid formation, AcCoA is used. This accounts for around 5% of the glucose carbon going to biomass. Finally around 10% glucose carbon is going to biomass precursors via citric acid cycle metabolites (replenished via the PEPCB reaction).

Maintenance. The calculated ATP hydrolysis flux allows to investigate the maintenance requirements for the strains. Figure 8 shows the energy requirements for different dilution rates. As with the other fluxes, the modified strains have really different maintenance requirements, indicating that there is no negative influence of the genetic modifications on the energy metabolism.

The growth associated maintenance is the slope of the line shown in Figure 8, while the non-growth-associated maintenance is found by taking the intercept of this line. For non-growth-associated maintenance, a value of 0.088 mol/molBM/h was

obtained. This conforms with the values reported in the literature for the wild-type: 0.20 mol/molBM/h (*38*) 0.073 mol/molBM/h (*39*), and 0.12 mol/molBM/h (*37*). The growth associated maintenance is 1.70 mol/molBM. In literature, both low values, 0.34 mol/molBm (*38*), and high values, 2.6 mol/molBM (*37*), can be found.

Conclusion

Three different approaches to minimize acetate formation were compared: (1) one approach that directly reduces carbon flow to acetate (3KO); (2) one approach that addresses underlying metabolic and regulatory mechanisms that lead to acetate formation (PPC); and one approach that combines the two strategies above (3KO-PPC).

Batch cultures under aerobic conditions were performed to evaluate these mutants compared to the wild-type. All approaches resulted in a decrease of about 20% of the growth rate. However, these mutant strains remain fast growing and, thus, suitable for application in large scale bioreactor processes.

Cutting off the carbon flow toward acetate (3KO) reduces the acetate yield significantly. On the other hand, the lactate yield increases substantially. The genetic approach of interrupting the carbon flow toward acetate results in minimizing acetate, but other byproducts are formed, making this strategy unfavorable. This confirms data found in the literature (*32*−*35*). The genetic approach of redirecting the carbon flow from PEP toward oxaloacetate (PPC) is more promising. The acetate and lactate yields decrease, whereas the succinate yield increases significantly. A combination of the two genetic approaches results in a similar behavior as replacing the natural *ppc* promoter by a strong promoter, except for the succinate yield that increases more.

For further characterization of the strains, chemostat experiments were conducted. Subsequently, the data of the chemostat experiments were used to perform metabolic flux analysis. The flux maps for the different strains showed no significant difference indicating no negative influence of the genetic modifications on primary metabolism. Also for the cellular energy metabolism (i.e., maintenance), no significant differences could be observed.

Taking into account the results of these batch cultures and MFA, the strain PPC can be used as a possible host for recombinant protein production. The genetic alterations in this strain show no unfavorable impact on primary metabolism and cellular energy metabolism. In addition, during batch cultures, more succinate is observed, indicating an increased flux toward the TCA cycle and, thus, toward the amino acid precursors.

Acknowledgment

The authors wish to thank the Institute for the Promotion of Innovation through Science and Technology in Flanders (IWT-Vlaanderen) for financial support in the framework of a Ph.D. grant (B/04316/01) to M. De Mey and for support via the Memore project (174WT105). The authors also wish to thank the Fund for Scientific Research-Flanders (FWO-Vlaanderen) for support (FWO-project G.0184.04). J. Maertens is a research assistant of the Fund for Scientific Research-Flanders (FWO-Vlaanderen).

References and Notes

(1) Nakano, K.; Rischke, M.; Sato, S.; Maerkl, H. Influence of acetic acid on the growth of *Escherichia coli* K12 during high-cell-density cultivation in a dialysis reactor. *Appl. Microbiol. Biotechnol.* **1997**, *48* (5), 597−601.

(2) Ko, Y.-F.; Bentley, W. E.; Weigand, W. A. A metabolic model of cellular energetics and carbon flux during aerobic *Escherichia coli* fermentation. *Biotechnol. Bioeng.* **1994**, *43* (9), 847−855.

(3) Eiteman, M. A.; Altman, E. Overcoming acetate in *Escherichia coli* recombinant protein fermentations. *Trends Biotechnol.* **2006**, *24* (11), 530−533.

(4) Datsenko, K. A.; Wanner, B. L. One-step inactivation of chromosomal genes in Escherichia coli K-12 using PCR products. *Proc. Natl. Acad. Sci. U.S.A.* **2000**, *97* (12), 6640−6645.

(5) Mashego, M. R. Ph.D. Thesis. Robust experimental methods to study in vivo pre-steady state kinetics of primary metabolism in *Saccharomyces cerevisiae*. TU Delft, 2005.

(6) Mashego, M. R.; van Gulik, W. M.; Vinke, J. L.; Heijnen, J. J. Critical evaluation of sampling techniques for residual glucose determination in carbon-limited chemostat cultures of *Saccharomyces cerevisiae*. *Biotechnol. Bioeng.* **2003**, *83* (4), 395−399.

(7) Theobald, U.; Mailinger, W.; Baltes, M.; Reuss, M.; Rizzi, M. In vivo analysis of metabolic dynamics in *Saccharomyces cerevisiae*: I. Experimental observations. *Biotechnol. Bioeng.* **1997**, *55*, 305−316.

(8) Ames, B. N.; Dubin, D. T. The role of polyamines in the neutralization of bacteriophage deoxyribonucleic acid. *J. Biol. Chem.* **1960**, *253* (3), 769−775.

(9) Gawronski, J. D.; Benson, D. R. Microtiter assay for glutamine synthetase biosynthetic activity using inorganic phosphate detection. *Anal. Biochem.* **2004**, *327*, 114−118.

(10) Lowry, O. H.; A., L. J. The determination of inorganic phosphate in the presence of labile phosphate esters. *J. Biol. Chem.* **1946**, *162*, 412−428.

(11) Lequeux, G.; Johansson, L.; Maertens, J.; Vanrolleghem, P. A.; Lidén, G. MFA for overdetermined systems reviewed and compared with RNA expression data to elucidate the difference in shikimate yield between carbon- and phosphate-limited continuous cultures of *E. coli* W3110.shik1. *Biotechnol. Prog.* **2006**, *22*, 1056−1070.

(12) Chen, R.; Yap, W. M. G. J.; Postma, P. W.; Bailey, J. E. Comparative studies of *Escherichia coli* strains using different glucose uptake systems: Metabolism and energetics. *Biotechnol. Bioeng.* **1997**, *56* (5), 583−590.

(13) Cozzone, A. J. Regulation of acetate metabolism by protein phosphorylation in enteric bacteria. *Annu. Rev. Microbiol.* **1998**, *52*, 127−164.

(14) Noronha, S. B.; Yeh, H. J. C.; Spande, T. F.; Shiloach, J. Investigation of the TCA cycle and the glyoxylate shunt in *Escherichia coli* BL21 and JM109 using ^{13}C NMR/MS. *Biotechnol. Bioeng.* **2000**, *68* (3), 316−327.

(15) Sauer, U.; Lasko, D. R.; Fiaux, J.; Hochuli, M.; Glaser, R.; Szyperski, T.; Wuthrich, K.; Bailey, J. E. Metabolic flux ratio analysis of genetic and environmental modulations of *Escherichia coli* central carbon metabolism. *J. Bacteriol.* **1999**, *181* (21), 6679−6688.

(16) Wick, L. M.; Quadroni, M.; Egli, T. Short- and long-term changes in proteome composition and kinetic properties in a culture of *Escherichia coli* during transition from glucose-excess to glucose-limited growth conditions in continuous culture and vice versa. *Environ. Microbiol.* **2001**, *3*, 588−599.

(17) Varma, A.; Palsson, B. O. Metabolic capabilities of *Escherichia coli*: II. Optimal growth patterns. *J. Theor. Biol.* **1993**, *165* (4), 503−522.

(18) Pramanik, J.; Keasling, J. D. Stochiometric model of *Escherichia coli* metabolism: incorporation of growth-rate dependent biomass composition and mechanistic energy requirements. *Biotechnol. Bioeng.* **1997**, *56* (4), 398−421.

(19) Karp, P. D.; Riley, M.; Paley, S. M.; Pellegrini-Toole, A. EcoCyc: An encyclopedia of *Escherichia coli* genes and metabolism. *Nucleic Acids Res.* **1996**, *24* (1), 32−39.

(20) Karp, P. D.; Riley, M.; Paley, S. M.; Pellegrini-Toole, A. The MetaCyc database. *Nucleic Acids Res.* **2002**, *30* (1), 59−61.

(21) Karp, P. D.; Riley, M.; Paley, S. M.; Pellegrini-Toole, A.; Krummenacker, M. EcoCyc: Encyclopedia of *Escherichia coli* genes and metabolism. *Nucleic Acids Res.* **1997**, *25* (1), 43−50.

(22) Karp, P. D.; Riley, M.; Paley, S. M.; Pellegrini-Toole, A.; Krummenacker, M. EcoCyc: Encyclopedia of *Escherichia coli* genes and metabolism. *Nucleic Acids Res.* **1998**, *26* (1), 50−53.

(23) Karp, P. D.; Riley, M.; Paley, S. M.; Pellegrini-Toole, A.; Krummenacker, M. EcoCyc: Encyclopedia of *Escherichia coli* genes and metabolism. *Nucleic Acids Res.* **1999**, *27* (1), 55−58.

(24) Karp, P. D.; Riley, M.; Saier, M.; Paulsen, I. T.; Collado-Vides, J.; Paley, S. M.; Pellegrini-Toole, A.; Bonavides, C.; Gama-Castro, S. The EcoCyc database. *Nucleic Acids Res.* **2002**, *30* (1), 56−58.

(25) Karp, P. D.; Riley, M.; Saier, M.; Paulsen, I. T.; Paley, S. M.; Pellegrini-Toole, A. The EcoCyc and MetaCyc databases. *Nucleic Acids Res.* **2000**, *28* (1), 56−59.

(26) Reed, J. L.; Vo, T. D.; Schilling, C. H.; Palsson, B. An expanded genome-scale model of *Escherichia coli* K-12. *Genome Biol.* **2003**, *4*, R54.

(27) Kanehisa, M.; Goto, S., KEGG: Kyoto Encyclopedia of Genes and Genomes. *Nucleic Acids Res.* **2000**, *28*, 27−30.

(28) Ogata, H. Kyoto Encyclopedia of genes and Genomes. *Nucleic Acids Res.* **1999**, *27*, 29−34.

(29) Lequeux, G.; Van der Heijden, R.; Van den Broeck, S.; Vanrolleghem, P. A. In *Computational methods to determine conserved moieties and parallel pathways in metabolic network models*, 9th IFAC conference on computer applications in biotechnology CAB9, Nancy, France, 2004; Nancy, France, 2004.

(30) De Maeseneire, S. L.; De Mey, M.; Vandedrinck, S.; Vandamme, E. J. Metabolic characterisation of *E. coli* citrate synthase and phosphoenolpyruvate-carboxylase mutants in aerobic cultures. *Biotechnol. Lett.* **2006**, *28* (23), 1945−1953.

(31) De Mey, M.; Maertens, J.; Lequeux, G. J.; Soetaert, W. K.; Vandamme, E. J. Construction and model-based analysis of a promoter library for *E. coli*: an indispensable tool for metabolic engineering. *BMC Biotechnol.* **2007**, *7*, 34.

(32) Contiero, J.; Beatty, C. M.; Kumari, S.; DeSanti, C. L.; Strohl, W. R.; Wolfe, A. J. Effects of mutations in acetate metabolism on high-cell-density growth of *Escherichia coli*. *J. Ind. Microbiol. Biotechnol.* **2000**, *24* (6), 421−430.

(33) El-Mansi, E. M. T.; Holms, W. H. Control of carbon flux to acetate excretion during growth of *Escherichia coli* in batch and continuous cultures. *J. Gen. Microbiol.* **1989**, *135* (11), 2875−2884.

(34) Yang, Y.-T.; Bennett, G. N.; San, K.-Y. Effect of inactivation of *nuo* and *ackA-pta* on redistribution of metabolic fluxes in *Escherichia coli*. *Biotechnol. Bioeng.* **1999**, *65* (3), 291−297.

(35) Dittrich, C. R.; Vadali, R. V.; Bennett, G. N.; San, K.-Y. Redistribution of metabolic fluxes in the central aerobic metabolic pathway of *E. coli* mutant strains with deletion of the *ackA-pta* and *poxB* pathways for the synthesis of isoamyl acetate. *Biotechnol. Prog.* **2005**, *21* 627−631.

(36) Farmer, W. R.; Liao, J. C. Reduction of aerobic acetate production by *Escherichia coli*. *Appl. Environ. Microbiol.* **1997**, *63* (8), 3205−3210.

(37) Carlson, R.; Srienc, F. Fundamental *Escherichia coli* biochemical pathways for biomass and energy production: identification of reactions. *Biotechnol. Bioeng.* **2004**, *85* (1), 1−13.

(38) Varma, A.; Palsson, B. Metabolic flux balancing: basic concepts, scientific and practical use. *Biotechnology* **1994**, *12*, 994−998.

(39) Kayser, A.; Weber, J.; Hecht, V.; Rinas, U. Metabolic flux analysis of *E. coli* in glucose-limited continuous culture. I. Growth-rate-dependent metabolic efficiency at steady state. *Microbiology* **2005**, *151*, 693−706.

Received May 25, 2007. Accepted July 20, 2007.

BP070170G